Black-Box Models for Laser Electrophotographic Printers – Recent Progress *

Yanling Ju [a], Tamar Kashti [b], Tal Frank [b], Dror Kella [b], Doron Shaked [c], Mani Fischer [c], Robert Ulichney [d], and Jan P. Allebach [a]
a: School of Electrical and Computer Engineering, Purdue University, West Lafayette, Indiana USA,
b: Hewlett-Packard Indigo, Ltd. Ness Ziona, Rehovot, 76101, ISRAEL,
c: Hewlett-Packard Laboratories Israel, Technion City, Haifa, 32000, ISRAEL,
d: Hewlett-Packard Laboratories USA, Andover, MA 01810, USA

Abstract

In the electrophotographic printing process, the deposition of toner within the area of a given printer-addressable pixel is strongly influenced by the values of its neighboring pixels in the digital halftone image. This interaction between neighboring pixels is complex and nonlinear. To account for these effects, a printer model can be embedded in the halftoning algorithm before the printing process. Models that are designed to predict the effect of these factors on the printed halftone page can be used to design halftoning processes that will yield higher print quality, more consistently.

In our previous work, we developed a strategy to account for the impact of a 5×5 neighborhood of pixels on the measured value of a printer-addressable pixel at the center of that neighborhood. We also examined the potential influence of a much larger neighborhood of pixels (45×45) on the central printer-addressable pixel. In the present paper, we improve the design of the test page for 45×45 pixel models to yield more accurate and more robust results with fewer pages. We create six different models to more accurately account for local neighborhood effects and the influence of a 45×45 neighborhood of pixels on the central printer-addressable pixel. These models have a variety of computational structures that allow system designers to choose the model that is best-suited to their particular application. They also offer varying degrees of accuracy. The model validation experimental results show that the best of these new models can yield a significant improvement in the accuracy of the prediction of the pixel values of the printed halftone image. With respect to prediction of mean absorptance (cross-validation), we gain over a 4× improvement in accuracy between the best of the six new models and our previous 5×5 model.

Introduction

Digital halftoning is the process of representing a continuous-tone image with a device that can render only two or a few different levels of absorptance. It is well known that the actual printed result may differ substantially from that which might be expected based on a simple point-to-point correspondance with the bitmap generated by the halftoning algorithm. The nature and source of these differences will vary depending on the marking technology – be it electrophotography or inkjet, and the specific characteristics of the print mechanism. With electrophotography, the deposition of toner within the area of a given printer-addressable pixel is strongly influenced by not just the halftone value at that pixel, but also by the halftone values of the immediately neighboring pixels. This local influence can be attributed to the fact that the spot size of the laser write beam is larger than a single printer-addressable pixel; the complex field interactions that are set up by the charge distribution on the photoconductor and in the toner in the gap between the photoconductor and the developer, and how this influences development; the further spreading of toner during the transfer and fusing processes; and optical scattering of incident light within the media. Models that are designed to predict the effect of these factors on the printed halftone page can be used to design halftoning processes that will yield higher print quality, more consistently.

The tabular equivalent grayscale model based on empirically determined parameters was first proposed by Pappas and Dong [1] in 1993. It has proven to be an effective means to deal with non-ideal printer behaviors. Pappas and Dong determined the parameters of their model via a macroscale approach. They printed specially designed halftone patches and measured the large-area average absorptance of these patches. They then solved a set of linear equations to determine the parameter values. Baqai and Allebach [2] determined the parameters of their tabular equivalent grayscale model via a microscale approach. For their 3×3 model, they printed all 512 instances of the binary halftone pattern of this size, and used fiducial marks to estimate the value of the center printer-addressable pixel within this 3×3 region. They then incorporated this model within the search-based direct binary search (DBS) algorithm. This type of model has also been successfully used to improve stochastic, dispersed-dot halftone image quality for inkjet printers [3].

The tabular equivalent grayscale model was extended to account for the influence of a larger 5×5 neighborhood on the printed absorptance of a given printer-addressable pixel with stochastic, dispersed-dot [4], and stochastic, clustered-dot [5] halftone textures. It was further extended [6] to account for the influence of an even larger 45×45 neighborhood that is intended to capture the effect of long-path scattering of light between the point where it is incident on the surface of the printed media and where it finally exits, known as the Yule-Nielsen effect [7]. More recently, a similar model was proposed to predict toner usage with dry toner laser EP printers [8]. We refer to all these models as *black-box models*, since they are based solely on measuring what is on the printed page, and do not incorporate any information about the marking process itself.

The present work is most closely related to our previous

*Research supported by the Hewlett-Packard Company, Palo Alto, CA.

work published in 2012 [6]. Here we improve the design of the test page for the 45×45 models to yield more accurate and more robust results with fewer pages. We describe six new models to more accurately account for local neighborhood effects and the influence of a 45×45 neighborhood of pixels on the central printer-addressable pixel. These new models are divided into three classes, and have a variety of computational structures that allow system designers to choose the model that is best-suited to their particular application. They also offer varying degrees of accuracy. Our target device in this paper is the HP Indigo Press 5000. However, the results should be broadly applicable to all electrophotographic printers. The remainder of the paper is organized as follows: We first introduce the test page design and the print-to-scan analysis procedure for new black-box models. Then, we review the structure of our prior 5×5 model ULM5×5 (Unbiased, Linear Model 5×5)[4, 5], and discuss in detail each of the six new models that we have developed. Next, we present experimental results for a selected set of these models. Finally, we provide conclusions based on the work described in this paper, and the results obtained with the seven models discussed herein.

Print-to-Scan Analysis for Black-Box Models

Throughout this article, we use $[m,n]$ for discrete spatial coordinates at the printer resolution and $[k,l]$ for discrete spatial coordinates at the scanner resolution. Their units are pixels. The function $g[m,n]$ denotes the discrete halftone image which is input to the printer. The function $s[k,l]$ denotes the scanned printed halftone, $\tilde{g}[m,n]$ denotes the printed halftone estimated from $s[k,l]$, and $\hat{g}[m,n]$ denotes the printed halftone predicted from $g[m,n]$ using one of our models. For each pixel of $g[m,n]$ the absorptance value can only take on values of 0 (white) or 1 (black), while each pixel of $s[k,l]$, $\tilde{g}[m,n]$, and$\hat{g}[m,n]$ has an absorptance value between 0 and 1.

Figure 1 shows the major steps in the print-to-scan procedure that we use to establish the relationship between the digital halftone sent to the printer and the average absorptance of each region corresponding to a single printer-addressable pixel in the scanned printed page. We print a set of specially designed test pages on an HP Indigo Press 5000 at a resolution of 812.8 dpi, and scan the printed pages using an Epson Expression 10000 XL scanner at a resolution of 2400 dpi. We then analyze these scanned images to generate the parameters for the seven models that are listed in Table 1. Figure 2 shows the single test page that can be

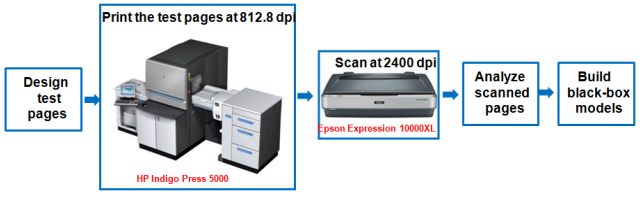

Figure 1. *Print-to-scan analysis procedure for the black-box models.*

used to directly estimate the parameters for Models-45×45 Class 2a - Class 3b in Table 1. We combine this single test page with those [6] used to generate ULM5×5 to generate Models-45×45 Class 1a and Class 1b. This particular test page is based on irregular, periodic clustered-dot halftone textures. It contains four distinct 101 × 101 pixel halftone patches corresponding to gray levels 4/255, 12/255, ..., 252/255, each printed 50 times. Each printer-addressable pixel within the 57 × 57 pixel center region has a surround of at least 45×45 pixels, and can be used to provide absorptance information for the 45×45 black-box models. For each of the 32 gray levels, there are $57 \times 57 \times 4 \times 50 = 649,800$ such pixels on the test page. By printing 50 replications of each digital halftone patch, we can characterize both the average behavior of the printer and the variation about that average due to intrinsic printer instability.

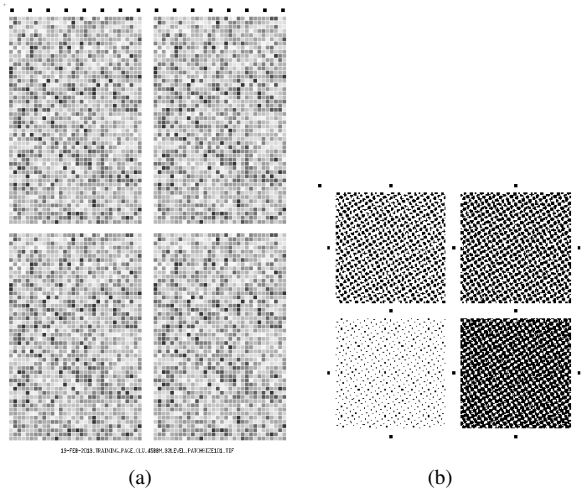

Figure 2. *(a) Test page for the 45×45 models, (b) Portion of test page for the 45×45 models. Each one of the four halftone squares in (b) corresponds to one of the small squares in (a). The fiducial marks in (b) are used to register the pixels in the scanned image of the printed test page to the pixels in the digital image sent to the press. Their size is 3×3 printer-addressable pixels.*

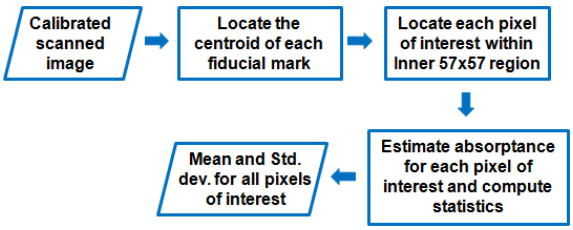

Figure 3. *Procedure for analysis of scanned printed test pages.*

Figure 3 shows the major steps for the scanned test page analysis, we first perform scanner gray balancing to calibrate the scanned pages to units of absorptance. We then estimate the center coordinates (here we use the centroid) for each fiducial mark. The centroid of each fiducial mark is calculated based on the spatial distribution of toner absorptance throughout its corresponding mask region. The horizontal and vertical centroids of the i-th segmented fiducial mark are given by Eq. (1).

$$C_{x,i} = \frac{\sum_{[k,l]\in D_i}(k-0.5)s[k,l]}{\sum_{[k,l]\in D_i} s[k,l]}, C_{y,i} = \frac{\sum_{[k,l]\in D_i}(l-0.5)s[k,l]}{\sum_{[k,l]\in D_i} s[k,l]}, \quad (1)$$

where D_i is the corresponding binary mask for the i-th fiducial mark in the binary mask image. The binary mask image is generated using the Otsu's method [9]. The parameter $s[k,l]$ is the absorptance value of the scanned image at the pixel with coordinates $[k,l]$. The 0.5 pixel offset in both parts of Eq. (1) shifts the effective coordinate location of each pixel to its center. For each 101×101 pixel halftone patch shown in Figure 2, we use the estimated centroid of the four adjoining fiducial marks to estimate the location of the center of each printer-addressable pixel in the scanned image, corresponding to one of the 57×57 pixels in the inner region of the digital halftone image that was sent to the printer. Let us consider the pixel at coordinates $[m,n]$ corresponding to the digital halftone value $g[m,n]$. Our target printer prints at 812.8 dpi; and we scan the images at 2400 dpi; so this printer-addressable pixel corresponds to a $2400/812.8 \times 2400/812.8$ region in the scanned image, where the units are scanner-addressable pixels. Since the center of this region will generally not be located at the center of a pixel in the scanned image; and the ratio $2400/812.8$ is not integer-valued, we use a sub-scanner-pixel procedure to estimate the average absorptance $\tilde{g}[m,n]$ corresponding to this printer-addressable pixel. Let $\Omega_{m,n}$ denote the set of $1/2400 \times 1/2400$ inch^2 scanner pixels $s[k,l]$ that overlap either wholly or partially with this region. In general, $\Omega_{m,n}$ will contain 16 pixels, as shown in Figure 4. We form the estimate $\tilde{g}[m,n]$ as a weighted sum of the pixels in $\Omega_{m,n}$, where the $[k,l]$-th weight $\omega_{m,n}[k,l]$ is equal to the fractional intersection of the region of the $[k,l]$-th scanner pixel with the $2400/812.8 \times 2400/812.8$ region centered at the location of the $[m,n]$-th printer-addressable pixel. This relationship is shown in Eq. (2).

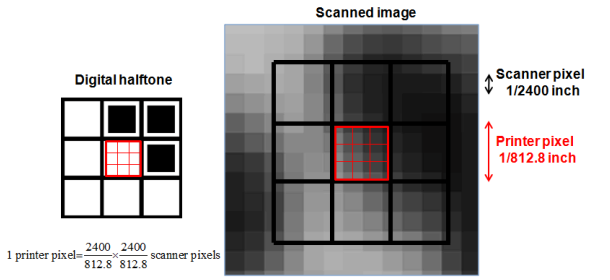

Figure 4. *Sub-scanner-pixel estimation of the absorptance of each printer-addressable pixel to account for misregistration between the printer and scanner lattices and the non-integer ratio of their resolutions.*

$$\tilde{g}[m,n] = \sum_{[k,l] \in \Omega_{m,n}} \omega_{m,n}[k,l] s[k,l]. \qquad (2)$$

After obtaining the absorptance of all pixels of interest, we estimate the sample mean $\tilde{g}$ and sample standard deviation $\tilde{\sigma}_g$ of the absorptance of each pixel of interest from the corresponding scanned printed halftone patches. We then can introduce the different structures, which will be described in the next section to model the influence of the neighborhood on the central pixel mean and standard deviation of absorptance.

Black-Box Models

The equivalent grayscale image $\hat{g}[m,n]$ summarize the effect of an $X \times X$ neighborhood of pixels in the digital halftone image on the printed absorptance of each printer-addressable pixel [2]. The equivalent grayscale image is defined to have the same average absorptance on a pixel-by-pixel basis as the actual printed halftone image. Under this assumption, we can express the discrete equivalent grayscale image in terms of a model Ω_{model} that account for the influence of this $X \times X$ neighborhood of pixels in the digital halftone image as

$$\hat{g}[m,n] = \Omega_{model}\{g[m+k,n+l],(k,l) \in [-K:K]^2\}, \qquad (3)$$

where $(2K+1) = X$, and $[-K:K]^2$ denotes the X^2 point set of 2-tuples formed by the cartesian product of $[-K:K]^2$ with itself, and Ω denotes the transformation of the binary value to the equivalent grayscale value of the center pixel. When K = 1, the printer model should predict the central pixel absorptance using the 3×3 neighborhood [2]. When K = 2, the neighborhood to be considered is 5×5 [4]. When K = 22, the neighborhood to be considered is 45×45 [6]. Figure 5 shows an example of how to use the printer model (Model-3×3) to generate the equivalent grayscale image.

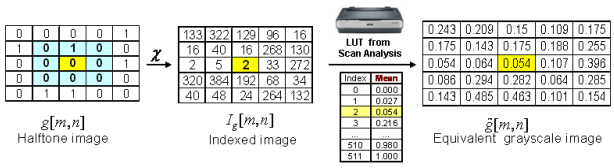

Figure 5. *Example of using Model-3×3 to generate the equivalent grayscale image.*

With electrophotography, the developed toner mass at any printer-addressable pixel in the image is a nonlinear function of the halftone in the neighborhood of that pixel. The black-box model is a tabular equivalent grayscale model based on the local dot configuration. It can be embedded into the halftoning algorithm for a more accurate result. For Model-3×3 [2], there are 512 (2^9) different 3×3 dot patterns. To ensure the full characterization of the printer for the 3×3 model, we designed test pages that include all 512 different dot configurations. We printed and scanned the test pages before doing any analysis; then analyzed the scanned test pages to estimate the mean and standard deviation of the central pixel absorptance for each 3×3 dot configuration. Specifically, our estimation of the mean and standard deviation of the central pixel absorptance for each 3×3 dot configuration were given by the sample mean and sample standard deviation of the corresponding scanned printed halftone patterns. We stored these estimated values in a lookup table (LUT) as Model-3×3.

We have a similar approach for the Model-5×5 [4]. We first used a 3×3 LUT to account for these interactions between dots [2]. And later, we presented an efficient strategy to estimate the impact of the 5×5 neighborhood pixels on the central pixel absorptance [4]. Instead of using all possible 5×5 dot profiles (2^{25}), we use a set of 160 different 5×5 outer rings with all possible 3×3 inner neighborhood to build Model-5×5. We assumed that dots in the outer ring of the 5×5 neighborhood have an additive influence on the central pixel absorptance. We followed the same LUT based approach as Model-3×3 to represent the influence of the inner 3×3 neighborhood; and we summarized the influence of the 5×5 outer ring by forming a weighted sum of these halftone pixels.

In our most recent paper [6], we described a 45×45 model: For each fixed 3×3 dot configuration, we measure the influence of the 45×45−5×5 outer neighborhood on the central pixel absorptance by summing the additional weighted contribution of each dot in the 5×5 ring and that of the 45×45−5×5 outer neighborhood. In the current paper, we improve the design of the test page for our 45×45 models to yield more accurate and more robust results with fewer pages. We chose different gray level halftone patterns as our dot configurations to collect the data for our 45×45 models. Using this strategy to choose dot configurations can keep the inner 5×5 dot configuration and the outer 45×45−5×5 neighborhood consistent.

In the current paper, we describe six new models that are divided into three classes, as shown in Table 1. The new models offer a variety of improvements over the previous models in terms of the number of free parameters, the number of test pages needed to parameterize the model, the number of computations required to predict each printed pixel value, and the model fit and prediction errors that can be achieved with the model. Each one of the six models has two different instantiations with identical structure, but different parameters. One is used to predict the average absorptance value at each printer-addressable pixel in the halftone image. The other is used to predict the standard deviation of the absorptance at that pixel. This latter statistic is used to characterize the stability with which a given local configuration in the halftone image can be printed. It is an intrinsic feature in the probabilistically-based direct binary search (DBS) algorithm that leads to more stable halftone textures, and thereby reduced grain and mottle [2, 3, 4, 5]. In addition, in this paper, we apply our models to irregular, periodic clustered-dot halftones. To our knowledge, this is the first time that a black-box model has been developed for irregular, periodic clustered-dot halftones.

We summarize the equations for the 45×45 models in Table 1. We use λ^* to denote the overall prediction of the central pixel absorptance for each specific black-box model, and use c_g^* as the constant weight term with gray level g. $\lambda_{i,j}^{5\times5}$ is the prediction using model ULM5×5 described in [4] and [5]. In the second step, we absorb the constant weight term within the weight vector to make a neat equation, which is good for least squares regression to determine the optimal weights.

Model-45×45 Class 1a and Class 1b are similar to the model presented in [6]. We combine the Model-45×45 training data with the ULM5×5. We assume that the dots in the 45×45−5×5 neighborhood have an additive influence on the central pixel absorptance, which is called correction weight term in this document. We consider two different approaches for the correction weight term. In the first approach, named Class 1a, the correction weight term is just a constant contribution of the 45×45−5×5 neighborhood depending on the gray level. In the second approach, named Class 1b, the correction weight term is a sum of the weighted contribution of inner 5×5 neighborhood and the constant contribution of the 45×45−5×5 neighborhood depending on its gray level.

Model-45×45 Class 2a and Class 2b are two lower dimensional models. We use only the measured absorptance values of the Model-45×45 training page to build these two models. To account for the influence of the inner 5×5 neighborhood on the central pixel mean and standard deviation of estimated measured absorptance, we optimize 25 weights for all the pixels within the inner 5×5 neighborhood. The difference between these two models is that for Class 2a, the 25 weights w^{2a} are gray level independent, while for Class 2b, the weights w_g^{2b} are gray level dependent.

Table 1: Computational structure of the black-box models.

Model	Equation	Neighborhood size
[1]ULM5×5	$\lambda_{i,j}^{5\times5} = \lambda_{i,0} + \psi_j^T w_i^{5\times5} + c_i^{5\times5} = \lambda_{i,0} + \Psi_j^T W_i^{5\times5}$	5×5
[2]M45×45 C1a	$\alpha_{i,j,g}^{1a} = \lambda_{i,j}^{5\times5} + c_g^{1a}$	45×45
[2]M45×45 C1b	$\alpha_{i,j,g}^{1b} = \lambda_{i,j}^{5\times5} + \psi_{i,j}^T w_g^{1b} + c_g^{1b} = \lambda_{i,j}^{5\times5} + \Psi_{i,j}^T W_g^{1b}$	45×45
[3]M45×45 C2a	$\alpha_{i,g}^{2a} = \psi_i^T w^{2a} + c_g^{2a} = \Psi_{i,g}^T W^{2a}$	45×45
[3]M45×45 C2b	$\alpha_{i,g}^{2b} = \psi_i^T w_g^{2b} + c_g^{2b} = \Psi_i^T W_g^{2b}$	45×45
[4]M45×45 C3a	$\lambda_{i_1,\ldots,i_4,g}^{3a} = \sum_{k=1}^{4} w_{i_k}^k + c_g^{3a} = \Psi_{i,g}^T W^{3a}$	45×45
[4]M45×45 C3b	$\lambda_{i_1,\ldots,i_5,g}^{3b} = \sum_{k=1}^{5} w_{i_k}^k + c_g^{3b} = \Psi_{i,g}^T W^{3b}$	45×45

[1] Here $\lambda_{i,0}$ is the measured central pixel absorptance of the i-th 3×3 dot configuration without the 5×5 ring, ψ_j denotes the dot distribution in the j-th 5×5 ring, and $w_i^{5\times5}$ are the weights corresponding to the dots in the 5×5 ring.

[2] Here i, j, and g are the indices of the 3×3 dot configuration, the 5×5 outer ring, and the gray level in the outer 45×45−5×5 neighborhood, respectively. $\psi_{i,j}$ states the dot distribution of the inner 5×5 dot configuration. We absorb the constant weight term within the weight vector by augmenting $\psi_{i,j}$ with a 1 to yield the vector $\Psi_{i,j}$.

[3] Here i and g are the indices of the 5×5 inner dot configuration and the gray level in the outer 45×45−5×5 neighborhood, respectively. ψ_i states the dot distribution of the inner 5×5 dot configuration.

[4] Here $i_1, i_2, i_3, i_4, and i_5$ are the indices of the five different 3×3 neighborhood located in the inner nerghborhood 5×5. $\Psi_{i,g}$ is a $(512\times K+32)\times 1$ vectors , where $K = 4$ (C3a), or 5 (C3b). The k-th block of 512 elements, $k = 1,\ldots,K$ contains a single 1 at the location indexed by i_k, and 0s elsewhere. Similarly, the final 32 locations contains a single 1 at the position corresponding to index of the average gray level in the outer 45×45-5×5 neighborhood quantized to the 32 levels in the training page.

For Class 3a and Class 3b, we introduce a totally different strategy to account for the influence of the inner 5×5 neighborhood on the central pixel mean and standard deviation of the estimated measured absorptance, by summing the contributions of four or five overlapping 3×3 neighborhoods, respectively, within the 5×5 neighborhood of the pixel to be predicted. To make these ideas a bit more concrete, as an example, we next describe Models-45 × 45 Class 3a and Class 3b in more detail. Figure 6 shows the structure of Model 45×45 Class 3a. This model separately looks at the binary halftone configuration within each of four different overlapping 3×3 neighborhoods located in the inner 5×5 neighborhood of the pixel whose value is to be predicted, and the average gray level within the outer 45×45−5×5 neighborhood to generate its predictions. From Figure 6, we may conclude that the model requires 6 table lookups, 2 multiplies, and 5 additions per pixel to predict either mean absorptance or the standard deviation of mean absorptance. This includes the computation required to perform the interpolation shown in the bottom left corner of Figure 6. For Class 3b we add the inner 3×3 as the fifth 3×3 neighborhood, and use five different 3×3 neighborhoods to better account for the influence of the inner 5×5 neighborhood on the pixel whose value is to be predicted. Since we have 512 differ-

Table 2: Summary of black-box model statistics.

Model	Description	No. of pages	No. of parameters	Computation per pixel*
ULM5×5	LUT indexed according to configuration of binary halftone within 3×3 neighborhood + 16 weights for outer ring + constant	6	9216	17 adds 16 muls
M45×45 C1a	ULM5×5 + gray-level-dependent† constant	7	9248 ‡	18 adds 16 muls
M45×45 C1b	ULM5×5 + 25 gray-level-dependent weights for inner 5×5 + gray-level-dependent constant	7	10048	43 adds 41 muls
M45×45 C2a	25 weights for inner 5×5 + gray-level-dependent constant	1	57	25 adds 25 muls
M45×45 C2b	25 gray-level-dependent weights for inner 5×5 + gray-level-dependent constant	1	832	25 adds 25 muls
M45×45 C3a	4 overlapping 3×3 LUTs in inner 5×5 region + gray-level-dependent constant	1	2080	4 adds
M45×45 C3b	5 overlapping 3×3 LUTs in inner 5×5 region + gray-level-dependent constant	1	2592	5 adds

†For all models, estimation of gray level is based on the average value of the digital halftone within 45×45−5×5 pixel outer region.
‡For all models with gray-level-dependent parameters, a separate parameter is used for each of the 256 gray levels.
*Number of additions (adds) and number of multiplications (muls).

ent 3×3 dot configurations for each 3×3 neighborhood, we need to optimize 512 × 4 weights for Class 3a, and 512 × 5 weights for Class 3b. And we still have one constant offset term for each gray level that we use in the training page to account for the influence of the outer 45×45−5×5 neighborhood on the center. The optimal weights for all these models can be estimated from the training data set by using a least squares method:

$$W^{optimal} = argmin\{\Psi^T W - \alpha\}, \\ = (\Psi^T \Psi)^{-1} \Psi^T \alpha. \quad (4)$$

Table 2 summarizes the parameters, number of test pages, and storage and computation required for each of the seven models shown in Table 1, and discussed above.

Experiments and Results

We provide experimental results for training our models with the irregular, periodic clustered-dot test page shown in Figure 2, printed with an HP Indigo Press 5000. We also test our black-box models with a different test page. This second page for model testing includes a set of 31 gray patches with gray levels located midway between those of the halftone patches that were used to train the model. So this is effectively a cross-validation procedure. We print and scan the test page. We then estimate the sample mean $\tilde{g}$ and sample standard deviation $\tilde{\sigma}_g$ of absorptance for each pixel of interest in the second test page using the same procedure as we did for the first test page that was used to train the models. We apply our black-box models to the digital testing page and compute the predicted absorptance $\hat{g}$ or standard deviation of absorptance $\hat{\sigma}_g$ for each pixel of interest in the test page. The prediction error here is the root mean squared error between the estimated measurement of absorptance $\tilde{g}$ or standard deviation $\tilde{\sigma}_g$ and the prediction $\hat{g}$ or $\hat{\sigma}_g$. It can state the predictive capability of our black-box models.

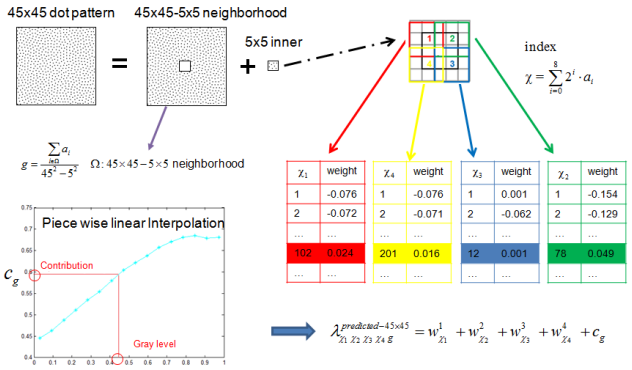

Figure 6. *Structure of Model-45×45 Class 3a that is used to predict both absorptance and standard deviation at a given printer-addressable pixel. The predicted value is the sum of five components. The first four components $w^k_{\chi_k}, k = 1,2,3,4$, are weights obtained from lookups into four different tables indexed according to the binary halftone patterns in each of the four overlapping 3×3 neighborhoods shown. Here χ_k is the index corresponding to the 3×3 binary neighborhood. The last component c_g accounts for the contribution of the average gray value in the surrounding 45×45-5×5 neighborhood. It is computed by interpolation between 32 values stored in a LUT, as shown in the lower left. All the model parameters are trained using the test page shown in Figure 2.*

Table 3 summarizes both the model-fit and cross-validation predictor performance averaged over 31 gray levels. The model fit error statistics are obtained by testing the predictors for mean absorptance and standard deviation of absorptance on the same data from the first test page that was used to train the models. The prediction error statistics are obtained by training the predictors on the first test page, and then testing them on data from the second test page. We see that in all cases the error decreases monotonically as we go from ULM5×5 to M45×45 C1b to M45×45 C3b. The model M45×45 C2a has the largest error since it has the fewest parameters. Also, the cross-validation errors are generally larger than the model-fit errors, as would be expected. With respect to prediction of mean absorptance (cross-validation), we gain more than a 4× improvement in accuracy between ULM5×5 and Model-45×45 Class 3b.

Figure 7 shows an example of the cross-validation model prediction images and prediction error images for mean absorptance using different black-box models. The example irregular, periodic clustered-dot halftone patch has an average gray level 96/255. The size of the image is 57×57 printer-addressable pixels. The prediction error images show the relative magnitude of the errors between the prediction and the measurement by identically scaling all three error images according to the largest mag-

Table 3: Model-fit and cross-validation prediction RMSE averaged over 31 gray levels*.

	Mean		Std. Dev.	
	Model-fit (%)	Cross-validation(%)	Model-fit (%)	Cross-validation(%)
ULM5×5	7.33	7.68	1.00	0.94
M45×45 C1a	3.77	4.17	0.91	0.89
M45×45 C1b	2.25	2.87	0.72	0.80
M45×45 C2a	5.06	4.77	1.52	1.31
M45×45 C2b	2.79	2.96	0.81	0.82
M45×45 C3a	1.83	2.17	0.70	0.70
M45×45 C3b	1.31	1.85	0.56	0.66

*All errors are in units of percent of maximum absorptance between 0 (white) and 100 (black). The gray levels span the range between 0 and 1.

nitude of error observed across the three error images. In keeping with the units of absorptance in which these images are shown, darker pixels in the prediction error images mean higher error. We can see from the prediction error images that ULM5×5 has the highest prediction error, and M45×45 Class 3b has the minimum prediction error, which is consistent with the statistics in Table 3 and the quality of the visual match between Figures 7(b) and 7(e).

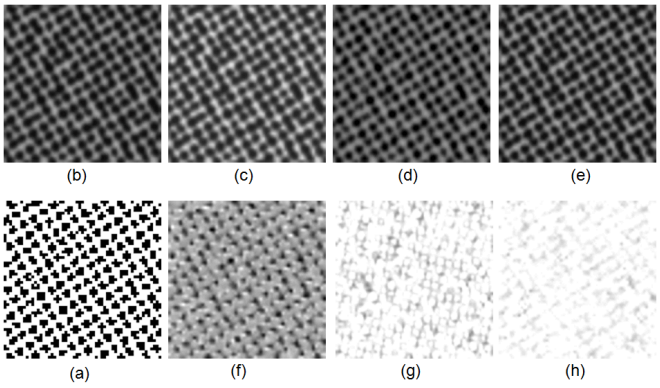

Figure 7. *Cross-validation model prediction images and absolute value error images for mean absorptance. The example clustered-dot halftone has an average gray level 96/255. (a) Digital halftone, (b) Estimated measurement, (c) ULM5×5 prediction, (d) M45×45 Class 2a prediction, (e) M45×45 Class 3b prediction, (f) ULM5×5 prediction error image, (g) M45×45 Class 2a prediction error image, (h) M45×45 Class 3b prediction error image. The three error images are computed by forming the absolute value of the error at each pixel, and then identically scaling the images to map the maximum across all three images to black and the minimum across all three images to white.*

Conclusions

In this paper, we improved the design of the test page for our 45×45 models to yield more accurate and more robust results with fewer pages. We describe six new models to more accurately account for local neighborhood effects and the influence of a 45×45 neighborhood of pixels on the central printer-addressable pixel. These new models are divided into three classes, and have a variety of computational structures that allow system designers to choose the model that is best-suited to their particular application. We applied our models to irregular, periodic clustered-dot halftones. We evaluated all the new models with printed halftone patches. The experimental results show that the extended models can yield a significant improvement in the accuracy of the prediction of the pixel values of the printed halftone image compared to our previous Model-5×5. With respect to prediction of mean absorptance (cross-validation), we gain over a 4× improvement in accuracy between the best new model (Model-45×45 Class 3b) and our earliest 5×5 model ULM5×5.

References

[1] T. N. Pappas, C. K. Dong, and D. L. Neuhoff, "Measurement of printer parameters for model-based halftoning," J. Electronic Imaging, Vol. 2, pp. 193-204 (1993).

[2] F. A. Baqai and J. P. Allebach, "Halftoning via direct binary search using analytical and stochastic printer models," IEEE Trans. on Image Processing, Vol. 12, pp. 1-15 (2003).

[3] J. H. Lee and J. P. Allebach, "Inkjet printer model-based halftoning," IEEE Trans. on Image Processing, Vol. 14, pp. 674-689 (2005).

[4] P. Goyal, M. Gupta, D. Shaked, C. Staelin, M. Fischer, O. Shacham, R. Jodra, and J. P. Allebach, "Electrophotographic model based halftoning," Color Imaging XV: Displaying, Processing, Hardcopy, and Applications, SPIE Vol. 7528, R. Eschbach, G. Marcu, S. Tominaga, and A. Rizzi, Eds., San Jose, CA, pp. 17-21 (2010).

[5] P. Goyal, M. Gupta, C. Staelin, M. Fischer, O. Shacham, T. Kashti, and J. P. Allebach, "Electro-photographic model based stochastic clustered-dot halftoning with direct binary search," Proc. IEEE International Conference on Image Processing, pp. 1721-1724 (2011).

[6] Y. Ju, D. Saxena, T. Kashti, D. Shaked, M. Fischer, R. Ulichney, and J. P. Allebach, "Modeling large-area influence in digital halftoning for electrophotographic printers," Color Imaging XVII: Displaying, Processing, Hardcopy, and Applications, SPIE Vol. 8292, R. Eschbach, G. Marcu, and A. Rizzi, Eds., San Francisco, CA, pp. 23-26 (2012).

[7] J. A. C. Yule, and W. J. Nielsen, "The penetration of light into paper and its effect on halftone reproduction," Tech. Assoc. Graphic Arts Proc. 3, pp. 6576 (1951).

[8] L. Wang, D. Abramsohn, T. Ives, M. Q. Shaw, and J. P. Allebach, "Estimating toner usage with laser electrophotographic printers," Color Imaging XVIII: Displaying, Processing, Hardcopy, and Applications, SPIE, Vol. 8652, R. Eschbach, G. Marcu, and A. Rizzi, Eds. San Francisco, CA, pp. 3-7, (2013).

[9] Mehmet Sezgin and Bülent Sankur, "Survey over image thresholding techniques and quantitative performance evaluation," J. of Electronic Imaging, Vol. 13, pp. 146-168 (2004)

Author Biography

Yanling Ju received her B.S. degree in electrical engineering from Peking University, Beijing, China, in 2006 and M.E. degree from the Graduate School of Chinese Academy of Science, China, in 2009. Now she is pursuing her Ph.D. in the School of Electrical and Computer Engineering, Purdue University, West Lafayette, IN. Her research interests are focused on signal and image processing, and printed image quality.